Zdzisław Bogdanowicz, Paweł Jóźwik, Barbara Nasiłowska

Microstructure and mechanical behavior of a CO_2 laser and TIG welded 904L steel

Struktura stali 904L spawanej wiązką lasera CO_2 i metodą TIG

Abstract

This paper presents the analysis of structural research, micro-hardness and mechanical properties of the base material which is steel 904 L and joints made with CO_2 laser beam and the TIG method. The analysis of the equilibrium system created in the Thermo-Calc programme based on chemical composition shows a dominancy of austenite with of Fe_α additions, phase σ, P and Laves' and $M_{23}C_6$ and $Cr_9Mo_{21}Ni_{20}$ carbides. EBSD (electron backscatter diffraction) research done by using an electron scanning microscope confirmed the presence of pure austenite.

Key words: steel 904L, welding, TIG, laser

Streszczenie

W pracy przedstawiono analizę badań strukturalnych, mikrotwardości i własności mechanicznych materiału rodzimego stali 904 L oraz połączeń wykonanych wiązką lasera CO_2 i metodą TIG. Analiza układu równowagi utworzonego w programie Thermo-Calc na podstawie składu chemicznego wykazała dominujący udział austenitu z domieszkami Fe_α, faz σ, P i Lavesa oraz węglików $M_{23}C_6$ i $Cr_9Mo_{21}Ni_{20}$. Badania EBSD (*electron backscatter diffraction*) wykonane przy użyciu elektronowego mikroskopu skaningowego potwierdziły obecność czystego austenitu.

Słowa kluczowe: stal 904L, spawanie, TIG, laser

1. Introduction

The object of the research is austenitic stainless steel 904 L (incl. percent. 24–26 ≤ Ni, Cr ≤ 19–21, Mo ≤ 4–5, Cu ≤ 1.2–2.0, Mn ≤ 2.0, N ≤ 0.15, Si ≤ 0.7, P ≤ 0.030, S ≤ 0.010, C ≤ 0.02) which was designed by Allegheny Ludlum Corporation for use in highly

Zdzisław Bogdanowicz Ph.D. Eng., Barbara Nasiłowska M.Sc. Eng.: Military University of Technology, Faculty of Mechanical Engineering; **Paweł Jóźwik Ph.D. Eng.:** Military University of Technology, Faculty of Advanced Technology and Chemistry; nasilowska.barbara@gmail.com

corrosive environments. The material is distinguished by a high stability of the austenite, which is not converted into martensite during nondifusion transformation in the wide range of temperatures and plastic deformation. The material shows a substantially greater resistance to corrosion, cracks, chemical corrosion, crevice and stress than conventional 300 series austenitic stainless steel. Despite the wide range usage of "super"-austenitic 904L steel in construction, refineries, nuclear power and chemical industry (Fig. 1), research of this material properties available in the literature is limited and there are just a few publications on this topic [1–3].
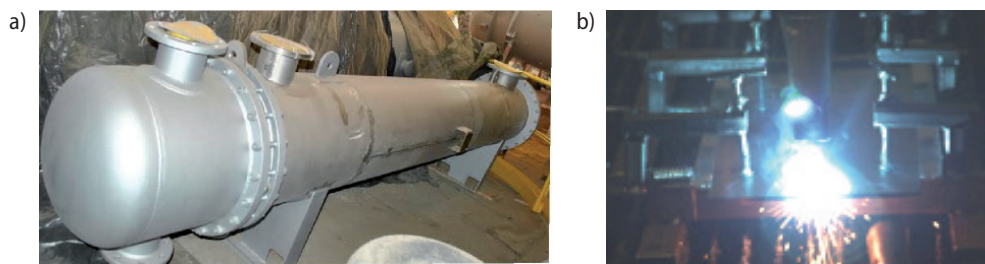
a)

b)

Fig. 1. Vapor condenser made of stainless steel 904L with TIG method [Department of Mechanical Chemical Equipment, Tarnów Azote Group] (a), laser welding of steel 904L (b)

2. The structure of the genuine material

The topography of grain orientation is more precise than optical microscopy and allows to determine the shape and size of grains [4]. An analysis of phase and crystallographic orientation of steel 904 L under the influence of dynamic deformations was presented in the article [5]. Research shows that the grains inside the transverse strands can result in little rotation while the transverse surfaces have less impact on the deformation texture. The average grain size is about 100 μm.

Electron backscattered diffraction (EBSD) research on the parent material structure of steel 904 L shows typical austenitic structure – numerous recrystallization twins nucleating at grain boundaries (Fig. 2a).
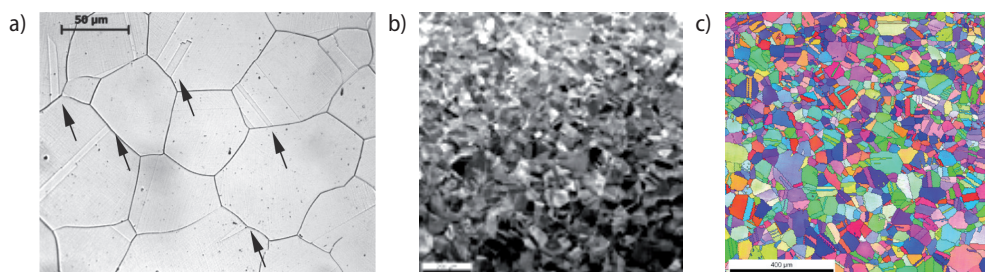
a)

b)

c)

Fig. 2. 904 L austenitic stainless steel parent material made at Nicon MA200 light microscope (a), by using the forward scatter detector (FSD) (b) electron backscatter diffraction EBSD (c)

Important parameter is the ferrite content in the steel on which corrosion resistance and tendency to crack during weld solidification depends. Ferrite content research performed on the 35 samples in the ZPMWIM at Warsaw University of Technology using FERRISCOPE MP30 shown purely austenitic structure. These results are confirmed by tests carried out using EBSD detector in the scanning microscope Quanta 3D FEG, which also shown a purity of austenic structure without the presence of residual ferrite and carbides. 904L stainless equilibrium system carried out in the temperature range from 0 to 1500°C depended on the content of nickel and other elements in the steel (Fe ≤ 49, Cr ≤ 19–21, Mo ≤ 4–5, Cu ≤ 1.2–2.0, Mn ≤ 2.0, N ≤ 0.15, Si ≤ 0.7, P ≤ 0.030, S ≤ 0.010, C ≤ 0.02) was made in the Thermo-Calc based on chemical composition, shows the dominance of austenite phase Feγ with the addition of σ, P and Laves' [6], $Cr_{23}C_6$ chromium carbides ($M_{23}C_6$) [7, 8], $Cr_9Mo_{21}Ni_{20}$ and residual ferrite Fe_α – Figure 3.
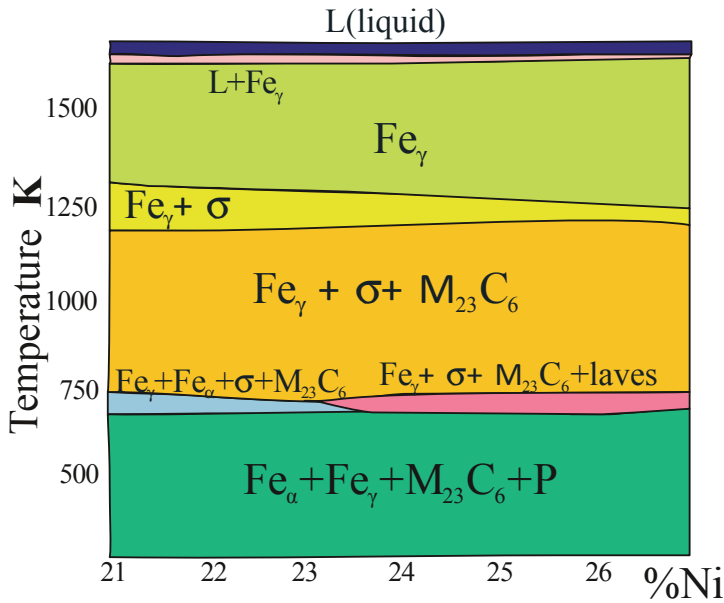

Fig. 3. 904L steel equilibrium system with varying nickel content

Sigma phase (FeCr) of the tetragonal structure is formed in the solid state by eutectoid transformation during slow cooling, affects inconveniently the properties of the material by increasing hardness (about 900 HV) and fragility [9]. Based on the equilibrium diagram of 904 L steel, the sigma phase may be released in the temperature range from 723 to 1323°C. Observations using SEM (EBSD), and research performed by using Shimadzu-Dorenst microhardness type "M" at a load of 0,981 N have not confirmed presence of this phase (Fig. 4).

Fig. 4. HV 0.1 genuine material microhardness research

Based on the results obtained in the Thermo-Calk for 904L steel, phase P may be in the form of a Cr-Fe-Mn and Cr below 723°C.

When the ratio of the atomic radius of two elements A (Cr) and B (Mo, Fe, Mn) is defined in the range of 1.05–1.68, AB_2-type Laves phases occurring in the alloy of Fe, Mn, Cr and Mo with other metals can appear. However, SE, EDS and EBSD research made with a scanning electron microscope also did not confirm the presence of the P and Laves' phase.

3. TIG and laser beam welds structure

Flat samples 250 × 500 × 5 mm were welded with the TIG method with tungsten non-melting electrode with diameter of 2.5 mm MTC MT-904L and G / W 20 25 5 CUL (20% Cr, 25% Ni, 4.5% Mo, 1.5% Cu) weld in the Department of Mechanical Chemical Equipment, Tarnów Azote Group according to their production technology.

The TIG joint made with three beads, flat front solidification with gradual of the overfusion of grain boundaries appeared Figure 5a. Under the influence of the thermal cycles in the join at the grain boundaries, small amounts of chromium carbides and eutectic of niobium occurred.

Longer heat stress and thereby slower solidification effected the growth of the lateral branches of the dendrites. Research of the joint structure made by TIG welds has implicated active dislocation pits and their tendency to form cracks DDC (Ductility Dip Cracking) at the grain boundaries during cooling in the solid state [6] Figure 5b.
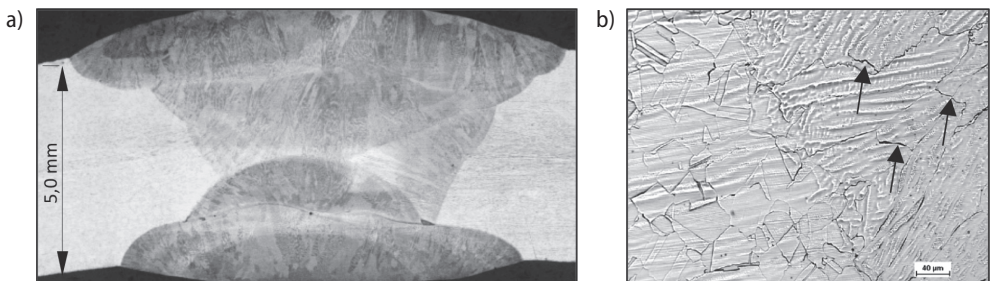

Fig. 5. TIG weld structure (a) and DDC crack appearance (b) observed using a light microscope

Figure 6 shows an image of a TIG welded joint, made by the forward scatter detector FSD and crystallographic orientation distribution map, using the inverse pole figure. An image of IPF (Inverse Pole Figure) shows the sample position in the direction of the reference system relative to the crystal lattice (Fig. 6). All grains of the same color correspond to uniform crystal orientation.

In austenitic steels, due to the heating solid-state dissolution of carbides in the austenite grain boundary occurs. As a result, the carbide precipitation reduces the intergranular corrosion resistance, due to decreasing of the cohesion between the grains of austenite, which results in the reduction of mechanical and plastic properties of steel.

Fig. 6. Joint microstructure obtained by using forward scatter detector (a) and electron backscattered diffraction (b)

In order to determine the width of the heat affected zone, microhardness tests, chemical composition measurement and EBSD analysis were carried out (Fig. 7), and showed a significant grain growth near the fusion line of 250 microns wide Figures 8a,b.

Whole weld area indicated the presence of austenite without intermetallic phases and carbides precipitates.
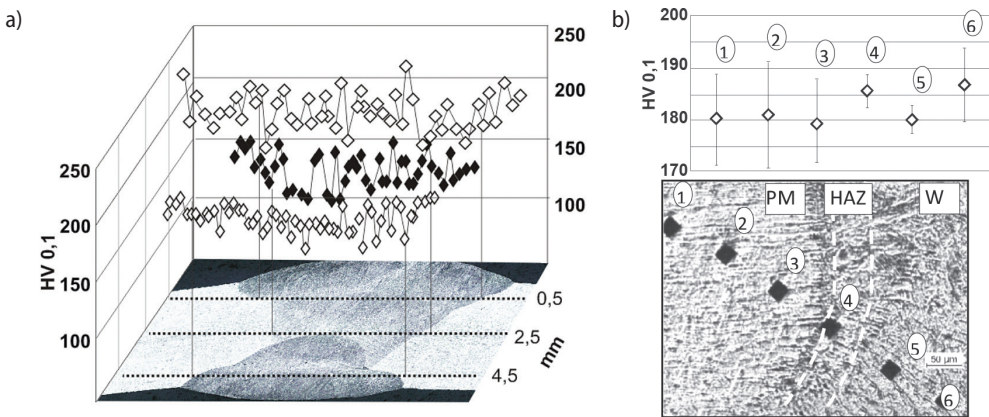

Fig. 7. Weld microhardness research (a) and heat affected zone of TIG welded joints (b)

Microhardness measurement on the metallographic surface of the TIG welds was conducted by the Vickers method in accordance to PN EN 1043-2-2000 norm with the indenter load of 100G (Fig. 8a) at 10 second and in the area of the fusion line (Fig. 8b). Research did not show significant changes in the microhardness of the analyzed areas. The average value of microhardness for TIG welded samples was 196 HV in the weld (S), 190 HV in the heat affected zone (HAZ) and (PM) 183 HV in the base material.
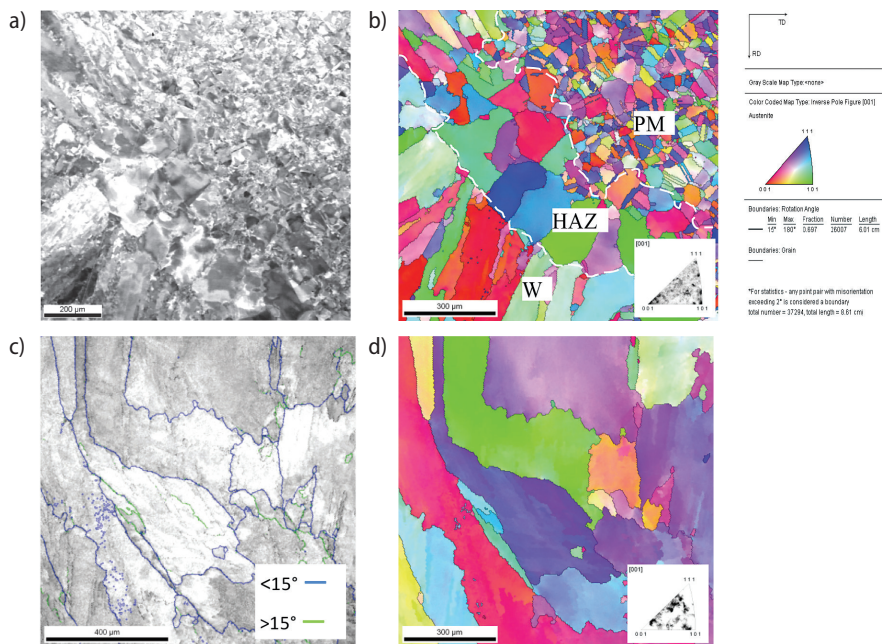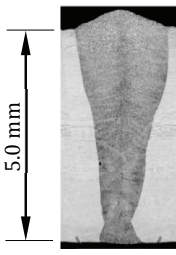

Fig. 8. Heat affected zone (a), (b) and joint (c), (d), made according to FSD (a), (c) and EBSD (b), (d) respectively

Choice of parameters for laser welding were performed at the focal lens distance of 270 mm on the sample surface spot of 0.4 mm diameter in the range; laser power $P = 4.0–5.0$ kW, welding speed $v = 0.8–2.2$ m/min, in helium atmosphere (Tab. 1). Flat samples $125 \times 500 \times 5$ mm were welded at the Laser Processing Research Centre at Kielce University of Technology using a CO_2 TRIUMF 1005 laser.

Selection of parameters for laser welding has been established in non-destructive testing (ultrasonic, radiographic and visual tests conducted in Mostostal Siedlce), and destructive tests (metallographic and microhardness measurements performed in the Department of Advanced Materials and Technology, New Technology and Chemistry Department at the Military University of Technology). Preparation of samples for metallographic investigations mainly included shape evaluation of the weld cap welded, edge of weld, and the presence of inclusions and blisters in the zone of the weld.

74

Table 1. Selection of the optimal parameters for laser welding (helium atmosphere)

P = 4.0 kW.				
v = 1.3 m/min	v = 1.4 m/min	v = 1.5 m/min	v = 1.6 m/min	v = 1.8 m/min
5.0 mm				

P = 4.5 kW						
v = 0.8 m/min	v = 1.0 m/min	v = 1.2 m/min	v = 1.4 m/min	v = 1.6 m/min	v = 1.8 m/min	v = 2.0 mmin

P = 5.0 kW						
v = 0.8 m/min	v = 1.0 m/min	v = 1.2 m/min	v = 1.4 m/min	v = 1.6 m/min	v = 1.8 m/min	v = 2.0 m/min

Focusing on the quality of the joints, the parameters of laser welding have been selected on the basis of the results of destructive testing, non-destructive and stress concentration. The following parameters for laser welding of 904L steel (marked in Table 1) were considered to be optimal: power laser beam P = 4.5 kW, feed rate of the laser beam v = 1.4 m/min; P = 5.0 kW, v = 1.0 m/min and P = 5.0 kW, v = 1.2 m/min.

In order to conduct the structural analysis which included phase analysis and gradiation (size and angle of the grain) EBSD research was performed using a scanning electron

microscope Quanta 3D FEG. An analysis of joint zone shows the fusion zone with column grains were predominant high angle boundary (Fig. 9, 10a,d). The EBSD observation did not show clear observation texture in analized zones (Fig. 10b,e).

Using EBSD research with contrasting local crystallographic orientation, the grain sizes were specified. Research has shown the greatest gradiation in the heat affected zone of TIG welds, while the lowest is in the heat affected zone in the joints made with a laser beam.

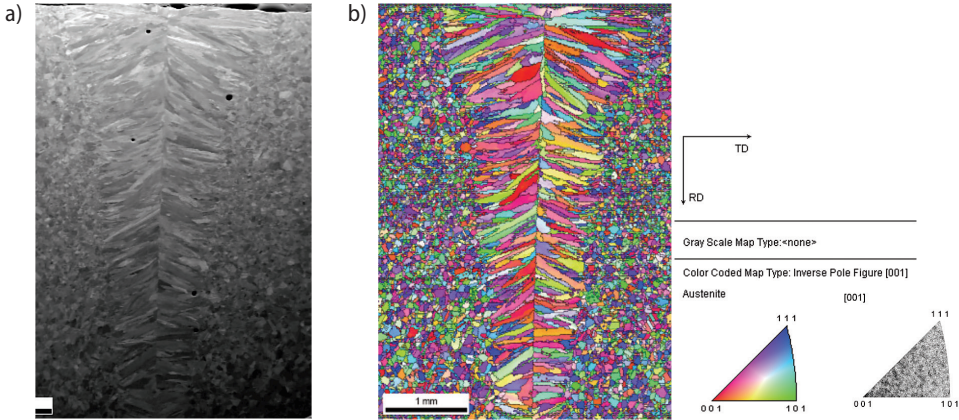Fig. 9. Laser beam welded joint structure (P = 4.5 kW, v = 1.4 m / min) under helium gas shield (a), (b)
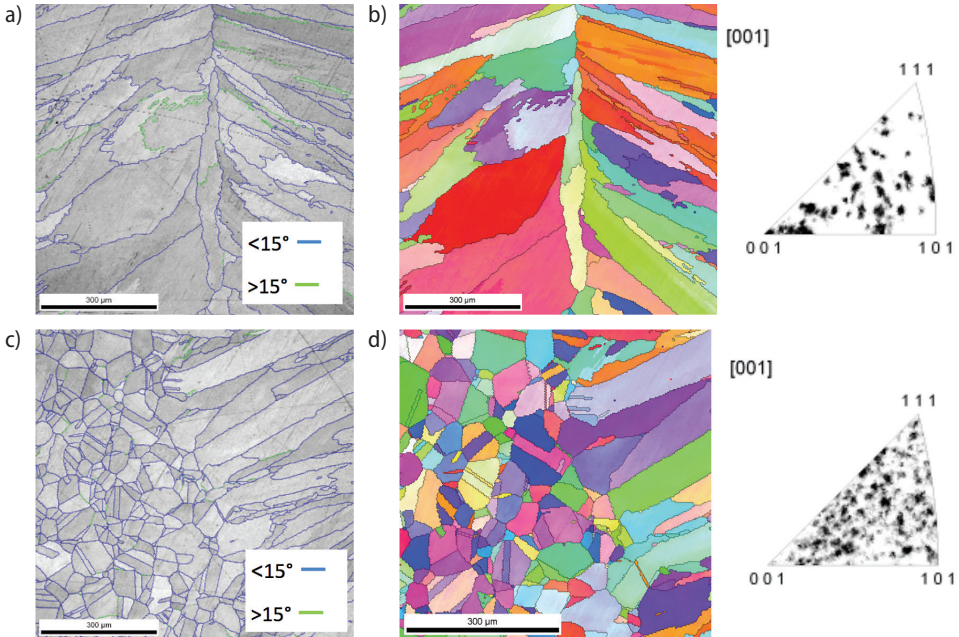

Fig. 10. Heat-affected zone (a), (b) and weld (c), (d), made respectively EBDS (a), (c) and EBSD (b), (d) using a scanning electron microscope

76

Microhardness measurement on the metallographic surface of the laser beam welds were conducted according to the Vickers method in accordance to PN-EN ISO 9015-2:2011 norm with the indenter load 100G (Fig. 11a) and the area of the fusion line (Fig. 11b).
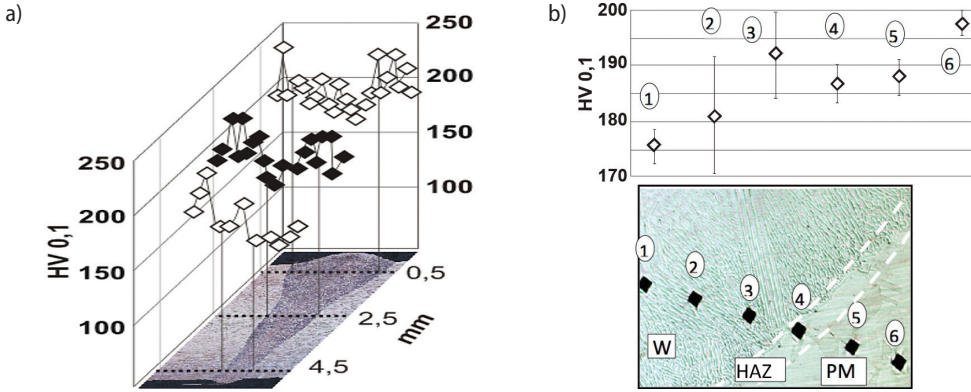

Fig. 11. Laser beam welded joints microhardness research (P = 4.5 kW iv = 1.4 m / min) (a) and heat affected zone (b)

The measurements showed no significant changes in the microhardness of the analyzed areas. The average value for the sample of micro-welded with a laser beam; was 201 HV in the weld (W), 189 HV in the heat affected zone (HAZ), and 185 HV in the parent material (PM).

4. Research of mechanical properties on welded joints

The mechanical properties of 904L austenitic stainless steel samples and TIG weld and laser weld were set on the INSTRON 8502 testing machine (Tab. 2) in accordance to PN-EN ISO 6892-1:2010.

Table 2. Mechanical properties of the parent material and the welds made using TIG and laser beam in relation to the normative values (average values)

	R_m [MPa]	R_{02} [MPa]	Z [%]	A [%]
Acc PN-EN 10027-8	**530–570**	**≥ 230**	**–**	**≥ 35**
Parent material	619	313	43	44.4
TIG weld	628	312	51	37.5
Laser weld	616	281	47	40.0

Fractures obtained in the static tensile test of flat parent material samples are characterized by a heterogeneous layered structure caused by hardening during rolling. With the progression of cervical narrowing, the fibers underwent to ductile fracture. Local material

shears show the ability of the material to significant plastic deformation in the analyzed welded joints. Fracture after the static tensile test TIG welded samples went through the recrystallized zone (Fig. 12). Microstructure was the same as that in the parent material.
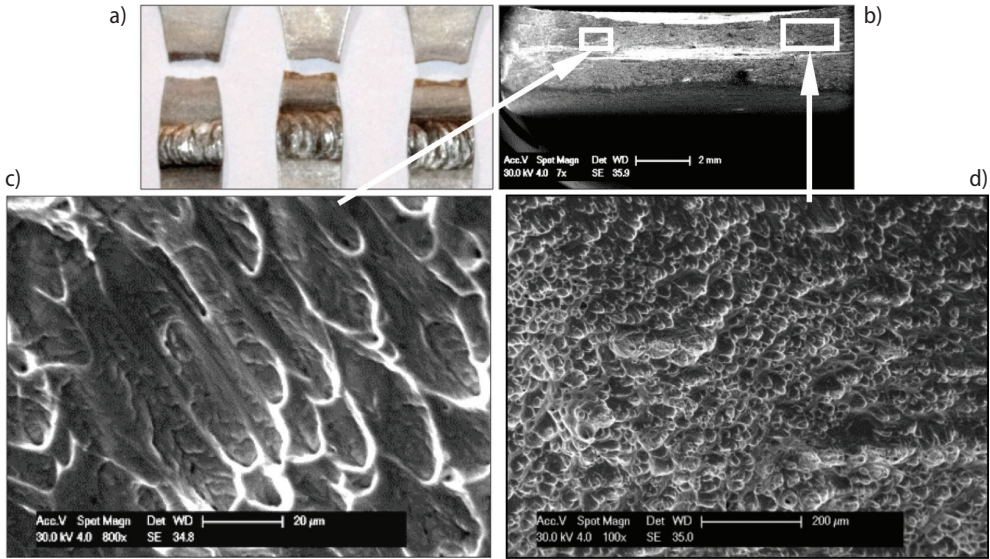

Fig. 12. Static fractures (a) and microstructure of the TIG welds after static tensile test (b), (c), (d)
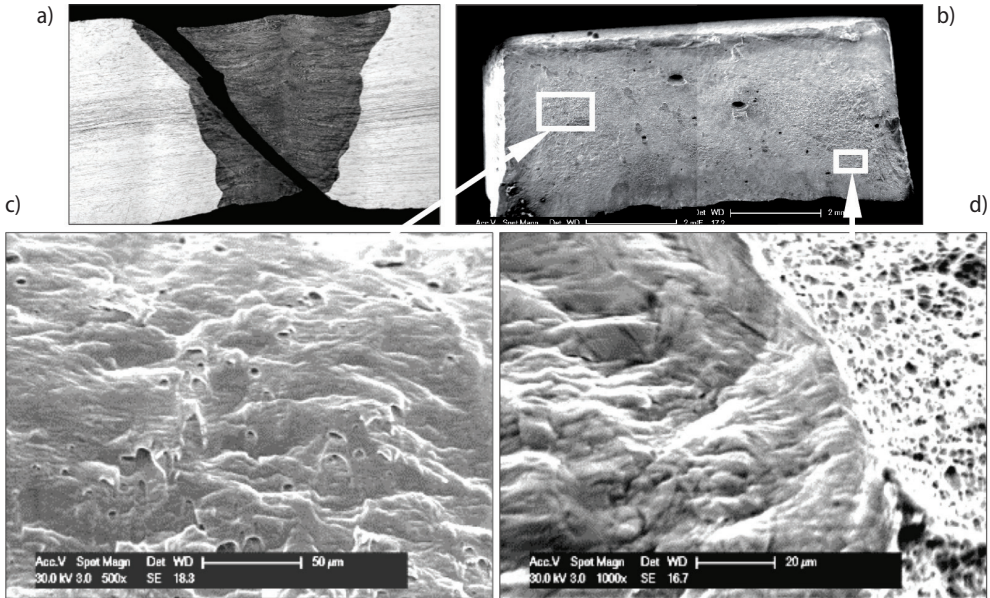

Fig. 13. Transverse metallographic of static fractures of the laser beam welded samples (a) and microstructure of laser-welded samples after static tensile test (b), (c), (d)

In the laser-welded joints static fractures occurred in the weld by passing through the fusion zone (Fig. 13).

In order to determine the mechanical properties of the main zones of welded joints, micro-samples from laser and TIG welded joints heat affected zones and the parent material were cut off by EDM and tested at hydraulic pulsator Instron 8501 (Fig. 14a,b).
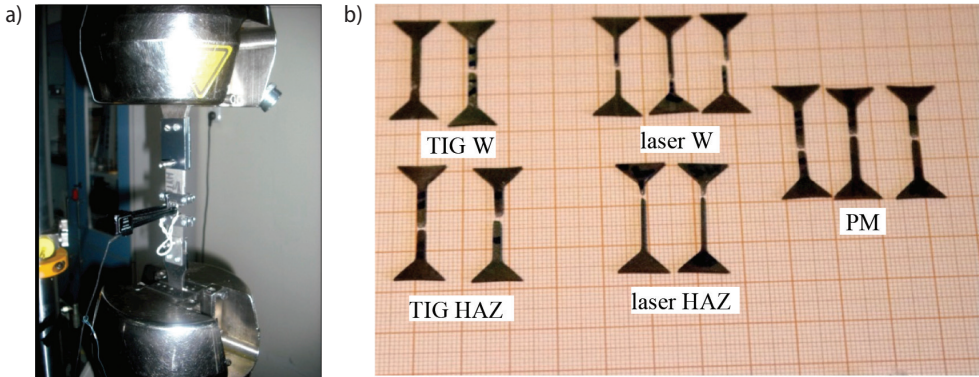

Fig. 14. Micro-sample static tensile test (a) and the samples after test (b)

Mechanical properties of the parent material and the TIG and laser welded joints with respect to the standard values are presented in Table 3.

Table 3. Results of the static tensile test of "micro"-samples cut from subsequent joint zones

	R_m [MPa]	R_{02} [MPa]	R_u [MPa]	Z [%]	A [%]
Acc PN-EN 10027-8	530–570	≥ 230	–	–	≥ 35
Genuine material	568	302	488	41	45.6
	571	310	565	45	40
TIG weld	606	387	623	38	39
	602	299	586	49	45
Heat affected zone TIG	523	296	541	45	43
	491	285	534	46	41
Laser weld P = 4.5 kW, v = 1.4 m/min	535	319	498	56	19
	537	326	540	65	22.5
Heat affected zone laser P = 4.5 kW, v = 1.4 m/min	533	276	528	48	33
	532	289	684	54	35

The Charpy impact test was performed with using Wolpert/Instron PW30 impact hammer with the blade instrumentation and the possibility of recording the breaking parameter changes. V-shaped samples were prepared in accordance with PN-EN 10045-1 and PE-EN ISO 14556 for the 1.4539 steel base material (PM), welds (W) and heat affected zone (HAZ) of laser beam and TIG method welds. In all of the tested samples delamination fracture occurred, what indicates a high degree of anisotropy of the material, caused by plastic working or by the presence of one or more bands of impurities, occurred [10] (Fig. 15). The results are presented in a bar graph of the amount of energy used to fracture the samples expressed in joules which is a measure of the impact (Fig. 15).
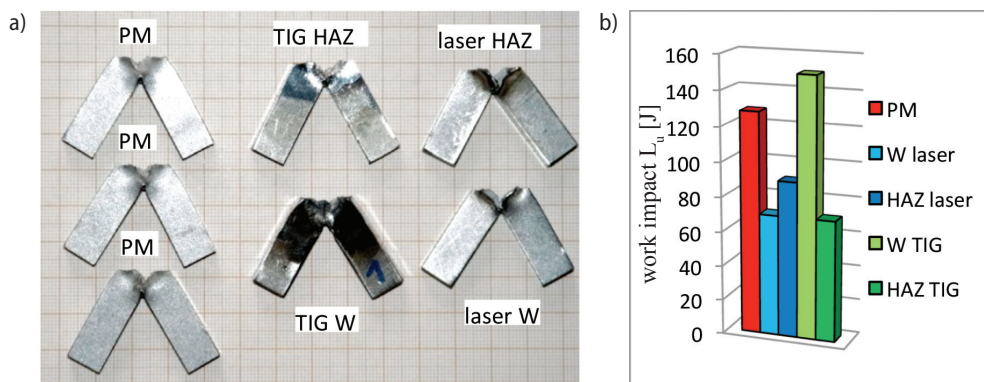

Fig. 15. Samples appearance after impact test(a) and energy used to break samples (b)

5. Summary

This study is the initial stage of a wider program of research on fatigue life of 1.4539 steel connections welded with laser and TIG method (dissertation).
1) Flat front of solidification with the melt-stage grain boundaries with a tendency to form cracks DDC was observed in the TIG weld.
2) In the weld node by the laser, transcrystalization with dendrites formation in the entire length of the fusion zone to the front line of heat dissipation was observed.
3) Analysed samples after welding (TIG and laser) presented ductile fracture. Fractures distribution of welded joints in a static tensile test for TIG weld occurred in the outside of the weld in the recrystallized zones, but for the laser method inside the weld. The TIG fusion zone surfaces after the crack show cup-cup fracture. The fracture by sheer was observed for samples after laser welding. Fractures in laser welded joints in the fatigue tests have been initiated in the fusion zone.
4) In all of the tested samples delamination fracture occurs what indicates a high degree of anisotropy of the material, caused by plastic working or by the presence of one or more bands of impurities.

References

[1] Report References Worldwide Erne Fittings GmbH, Hauptstraße 48, 6824 Schlins, Austria/Europe, 2008, http://ernefittings.com/ [access: 16.12.2013]

[2] Swindeman R. W.: Fatigue of austenitic stainless steels in the low and intermediate cycle range. Metals and Ceramics Division, Contract No. w-7405-eng-26, 1966

[3] http://nickelinstitute.org/ [access: 25.02.2014]

[4] Piątkowski A.: Badanie struktury materiałów metodą dyfrakcji elektronów wstecznie rozproszonych (EBSD). http://www.labportal.pl [access: 7.05.2014]

[5] Li N., Wang Y.D., Lin Peng R., Sun X., Ren Y., Wang L., Cai H.N.: Synchrotron X-Ray Diffraction Study of Texture Evolution in 904L Stainless Steel under Dynamic Shock Compression. The Minerals, Metals & Materials Society and ASM International, Metallurgical and Materials Transactions A, 42, 1 (2011), 81–88

[6] Błachowski A.: Wpływ domieszek, mikrostruktury i temperatury na kinetykę przemiany fazowej α–σ w układzie Fe-Cr. Rozprawa doktorska. Kraków, AGH, Wydział Fizyki i Techniki Jądrowej, 2009

[7] http://thomas-sourmail.net/stainless/ [access: 12.01.2014]

[8] Penga B., Zhanga H., Hongb J., Gaob J., Zhanga H., Wanga Q., Li J.: The effect of M23C6 on the high-temperature tensile strength of two austenitic heat-resistant steels: 22Cr-25Ni-Mo-Nb-N and 25Cr-20Ni-Nb-N. Materials Science and Engineering A, 528, (2011), 10–11

[9] Sathiya P., Panneerselvam K., Abdul Jaleel M.Y.: Measurement of the bead profile and microstructural characterization of a CO_2 laser welded AISI 904L super austenitic stainless steel. Optics & Laser Technology, 42 (2010), 960–968

[10] Katarzyński S., Kocańda S., Zakrzewski M.: Badanie własności mechanicznych metali. Warszawa, PWT, 1961